Weak interactions in Graphane/BN systems under static electric fields—A periodic ab-initio study

Lukas Eugen Marsoner Steinkasserer, Nicola Gaston, and Beate Paulus

Citation: The Journal of Chemical Physics **142**, 154701 (2015); doi: 10.1063/1.4917170
View online: http://dx.doi.org/10.1063/1.4917170
View Table of Contents: http://scitation.aip.org/content/aip/journal/jcp/142/15?ver=pdfcov
Published by the AIP Publishing

Weak interactions in Graphane/BN systems under static electric fields—A periodic *ab-initio* study

Lukas Eugen Marsoner Steinkasserer,[1,2,a)] Nicola Gaston,[2] and Beate Paulus[1]
[1]*Institut für Chemie und Biochemie, Freie Universität Berlin, Takustraße 3, 14195 Berlin, Germany*
[2]*MacDiarmid Institute for Advanced Materials and Nanotechnology, School of Chemical and Physical Sciences, Victoria University of Wellington, P.O. Box 600, 6140 Wellington, New Zealand*

(Received 20 January 2015; accepted 27 March 2015; published online 16 April 2015)

Ab-initio calculations via periodic Hartree-Fock (HF) and local second-order Møller-Plesset perturbation theory (LMP2) are used to investigate the adsorption properties of combined Graphane/boron nitride systems and their response to static electric fields. It is shown how the latter can be used to alter both structural as well as electronic properties of these systems. © *2015 AIP Publishing LLC.* [http://dx.doi.org/10.1063/1.4917170]

I. INTRODUCTION

In the wake of the experimental realization of Graphene by Geim and Novoselov in 2004[1] and the growing interest in the subject over the past years,[2] the study of so-called 2D-materials has seen a rapid rise in both experimental as well as theoretical science. While originally motivated by Graphene's exceptional mechanical and electronic properties,[3] the discovery and rediscovery of many other 2D-materials holds considerable promise for future applications in a variety of fields.[4]

Two materials which have found themselves at the forefront of this effort are Graphane (a fully hydrogenated form of Graphene) as well as hexagonal boron nitride (BN). While the use of BN as a lubricant has been widespread since the 1940's,[5] it has only recently emerged as a possible substrate for Graphene-based nanoelectronics[6–11] and other nanoscience applications. Graphane on the other hand has been the subject of a number of computational studies[12–14] before being only rather recently realized experimentally for the first time in 2009.[15] Its relatively short history notwithstanding, Graphane has proven to be an interesting material[15] due to its large hydrogen content and the presence of a finite band gap[12] not observed for pristine Graphene.

It is the presence of these, considerably sized, band gaps (6.0 eV for BN[16] and 6.17 eV for Graphane[17]) that make Graphane and BN interesting materials as dielectrics in electronic applications. On top of this, doping of Graphane has been proposed as a method for its use in transistor applications[18] as the substance is predicted to exhibit a good conduction behavior if the problem of the large band gap can be overcome.[19] On the other hand, BN has further been proposed as a potentially useful hydrogen-storage material and external electric fields have been predicted by theoretical investigations to be very useful in controlling the bonding strength of molecular hydrogen to a BN substrate.[20] Aside from these prospects for the use of single BN or Graphane sheets, multi-layering of different substances provides an avenue for combining their properties in useful ways. The use of external electric fields can further provide a way of reversibly controlling these properties from the outside, which leads to a wide variety of possible real world applications.

For all these reasons, the study of the combined Graphane/BN systems and in particular their response to external electric fields is of great interest and insights might well be gained from their detailed understanding. The systems are made even more appealing by the delicate interplay between van-der-Waals (vdW) forces which dominate the binding and static repulsive interactions. The former present great challenges to theoretical investigations and are in fact not adequately described by standard density functional therory (DFT) methods. The present systems further present the difficulty that the effects of an external electric field have to be accounted for as accurately as possible.

Post-Hartree-Fock (post-HF) methods using local second-order Møller-Plesset perturbation theory (LMP2) have just recently for the first time been successfully applied to the problem of multi-layering of Graphane and hydrogenated BN nanostructures,[21] and this work extends the previous research on molecular adsorption processes of H_2O on Graphene[22] and N_2 on BN monolayers[23] as well as crystalline BN bulk properties.[24,25] Since these methods do not involve any fitted parameters, they are exceptionally well suited for gaining theoretical insights into the details of the interactions in Graphane/BN heterostructures. The MP2 method further has the advantage of enabling the inclusion of electric field effects (via the HF-wave function) into the computation of vdW-interactions. The methods employed in this work further allow for the simulation of true 2D-periodic structures and therefore the application of a constant external electric field perpendicular to the system, without the need to achieve zero net-field within a unit cell. Herein we present, to the best of our knowledge, the first *ab-initio* post-HF investigation of Graphane/BN combined systems, including the effects of a constant, external electric field, applied perpendicularly to the Graphane/BN-plane.

a)marsoner@zedat.fu-berlin.de

II. COMPUTATIONAL DETAILS

Periodic HF-calculations were performed using the CRYSTAL09 program[26,27] while LMP2 calculations were carried out using the CRYSCOR09[28–30] code. The term "interaction energy" will be used throughout this work and refers to the BSSE-corrected interaction energy between the components of the layered systems. For a system AB, comprised of subunits A and B, it is defined as $E_{int} = E(AB) - [E(A)^* + E(B)^*]$, where E_{AB} is the energy of the AB-system and E_A^*/E_B^* are the energies of the individual subsystems calculated using ghost functions. Our method differs slightly from the standard counterpoise correction as proposed by Boys and Bernardi[31] in that isolated sheets of BN/Graphane, respectively, are calculated within a symmetrical set of ghost layers of Graphane/BN (see supplementary material for details[32]). This avoids shortcomings arising from the asymmetrical basis set augmentation as caused by the ghost functions during the counterpoise correction which leads to artifacts in the potential energy curves when an external electric field is applied. The basis set used was based on the aug(d,p)-6-31G** basis set used by Tanskanen *et al.*[21] As the inclusion of electric field effects made the use of the dual basis set scheme employed by Tanskanen *et al.* impossible, the exponents for d-type functions of B and N were reoptimized. The resulting basis set is given in the supplementary material.[32] As MP2-calculations are known to necessitate an accurate description of the virtual space, ghost functions have been added to both sides of all systems considered in this work with the details again provided in the supplementary material.[32] Note that the effect of augmenting the virtual space by adding ghost functions is small. For the S4 system at its equilibrium distance, for example, the difference in interaction energy is only 1.8 meV/unit cell (at the LMP2-level) indicating the quality of the aug(d,p)-6-31G** basis set for the calculations performed herein. For the LMP2 calculations, pair cut-offs of 6.0 and 12.0 Å for weak and distant pairs, respectively, were used (see CRYSCOR manual for details). The virtual space definition was done in two steps: First, a calculation using the Boughton Pulay criterion[33] with the tight (0.9965) threshold was applied to one of the studied systems. This domain definition was chosen as a reference, as it provides 10-atom domains for the non-bonding BN Wannier functions (WFs), in accordance with those used in the literature.[23,24] In order to achieve consistent domains for all calculations, in a second step this setting was then used to define domains according to WF-distance across all systems. More details on the CRYSTAL and CRYSCOR computational parameters are given in the supplementary material.[32] For interlayer distance scans, integral classification was performed on the system with the smallest interlayer distance and kept fixed during the scan. The excitation domains, WF-pairs, and the number of projected atomic orbitals were also held constant, following the procedure described by Usvyat.[30] Graphane structures used in this work were obtained from bulk-Graphane (Space group $P\bar{3}$ m1 (164)) for which the in-plane lattice constant was fixed to the experimental h-BN lattice constant (2.5038 Å),[34] and the positions of the H and C atoms were allowed to relax. BN structures on the other hand consisted of completely planar sheets at the same experimental lattice constant. All structural relaxations were performed at the PBE0/pob-TZVP-level.[35,36] Note that the mismatch between the PBE0/pob-TZVP-relaxed Graphane lattice constant and the experimental BN lattice constant is only 0.6%.

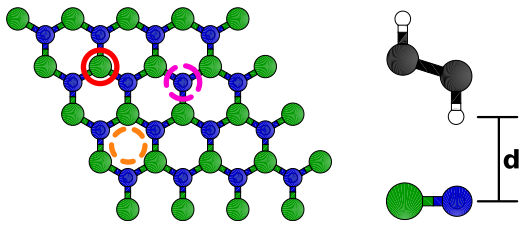

FIG. 1. The left-hand image shows the high-symmetry adsorption sites on a BN monolayer as colored circles, while in the right-hand figure, the definition of the interlayer spacing used throughout this work has been indicated. Note that the definition is analogous in the BN/Graphane/BN trilayer case. Carbon atoms are shown in black, hydrogen atoms in white, and boron atoms in blue while nitrogen atoms are indicated in green.

III. RESULTS AND DISCUSSION

A. Structural properties

As a starting point let us first consider all different high-symmetry adsorption situations for Graphane on BN. The three adsorption sites shown on the left-hand side of Figure 1 result in a total of six different adsorption-situations for Graphane on BN which can be pictured as being obtained via subsequent 60° rotations of one of the two layers. A graphical illustration of this procedure as well as a schematic representation of all six high-symmetry adsorption situations is shown in Figure 2 which further gives the naming scheme used throughout this work.

The first question which arises naturally is the relative stability of different adsorption situations. For weakly bound systems, these often tend to be very close in energy with only small potential barriers between them, which in turn provides a challenge to automated structure optimization algorithms. In Figure 3, we have shown potential energy surface (PES) plots for all six Graphane/BN bilayer systems. The curves are broadly divisible into two groups, with the systems termed S1 and S4 displaying considerably stronger binding than the

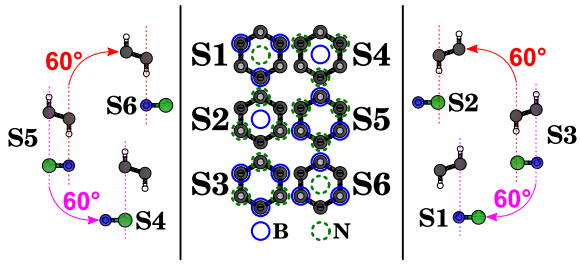

FIG. 2. The central image shows a top-view of the six high-symmetry adsorption situations for the Graphane/BN bilayer system. The BN-layer has been removed for clarity and the B- and N-positions indicated instead by colored circles only. Side views of the same structures as well as the rotations interconnecting them are shown on the right- and left-hand site. Carbon atoms are shown in black, hydrogen atoms in white, and boron atoms in blue while nitrogen atoms are indicated in green.

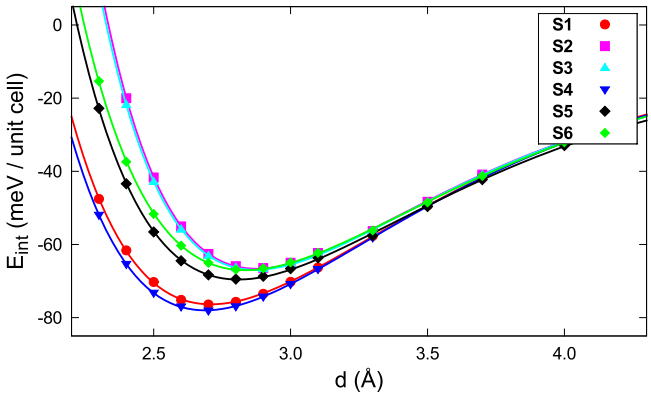

FIG. 3. PES at the LMP2-level for all Graphane/BN bilayer systems considered in this work. The naming scheme is the same as defined in Figure 2.

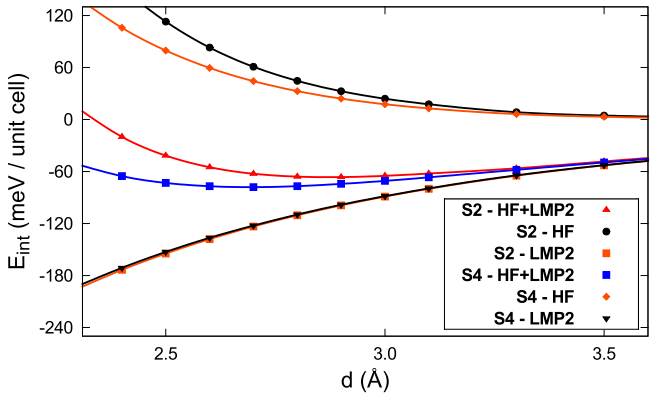

FIG. 4. HF and LMP2 contributions to the potential energy curves of the S2 and S4 system. For clarity the total curve, i.e. $E_{HF} + E_{LMP2}$ is also shown.

other four curves. Upon referring to Figure 2 we see that these two configurations are characterized by the Graphane H-atom being adsorbed at the hollow-side (orange circle in Figure 1).

The two curves not only show stronger adsorption energies than the remaining ones by ≈9–10 meV/unit cell but also slightly shorter equilibrium distances of about 2.7 Å as compared to the 2.8–2.9 Å seen for the other systems. While all curves in the two groups basically overlap for distances larger than ≈2.9 Å and indeed all coincide around distances of ≈3.5 Å, the behavior for smaller interlayer distances differs between different systems and provides some insight into the details of the interaction.

Considering again the S1/S4 pair, we see that the S4 system shows stronger interlayer binding than the S1 system. By comparing to the analogous behavior of the S5/S6 systems (which share a common B-adsorption site), this difference in behavior can be traced to the position of the N-atom which in the S1 and S6 cases is adsorbed in the hollow-site, while it is on top of the lower-lying carbon in the S4 and S5 cases. The reason for the difference now lies in the fact that, while there is only one nearest-neighbor lower-lying carbon atom in the S4 and S5 cases, their number rises to three in the S1/S6 case. At the same time the distances between the N atom and its nearest-neighbor lower-lying carbon for the S1 and S4 systems differ by only ≈0.2 Å at their equilibrium distance. This importance of the N-atom position further helps to explain the fact the S2/S3 pair of systems shows virtually no difference in energy as they both share a common N-adsorption site.

Having now analyzed the origin of the difference in binding behavior between the different adsorption situations, the question naturally arises as to what is the relative role of dispersive and static interactions to the binding. The aforementioned importance of the N-atom position, especially relative to the close-lying H-atom, suggests that the preference for specific adsorption sites might be mainly a steric effect, dominated by the negatively charged N-atom in the BN-layer.

To verify whether this is indeed the case, we have plotted in Figure 4 the respective contributions of the HF and the LMP2-energy to the interlayer binding in the S2 and S4 systems. While the S4 system shows the strongest binding, binding is equal within the error of the calculations for the S3 and S2 systems. We have chosen the S2 system as a comparison as it gives us the further advantage of allowing to isolate the effect of the N atom position as both systems share the same B adsorption site. Given the very small difference between the two LMP2 correlation-energy curves, the difference between the two structures is evidently caused by the HF-contribution to the binding which in both cases is purely repulsive, eliminating the option of possible BN-Graphane interlayer hydrogen bonding. The curves further help to emphasise the above-mentioned strong influence of the N–H interaction on binding as the repulsive HF part rises much more strongly in the S2 case than in the S4 case in accordance with stronger steric repulsion in the former as compared to the latter.

After having analyzed in some detail the Graphane/BN binding, we will now consider the effects of introducing a second BN layer, creating a BN/Graphane/BN trilayer structure. This is both interesting on a theoretical basis as a further study of vdW effects in multi-layered structures, as well as of possible practical use. Even though, as mentioned in the introduction, the band gap of pure Graphane is likely too large for electronic applications; doping of Graphane might well render it a viable channel-material and even with our BN/Graphane/BN model being a very simplified model system of possible real-live Graphane transistors, insights gained from the current investigation should still help to better understand more complicated structures in the future.

A structural model of the BN/Graphane/BN trilayer is shown in the inset of Figure 5. The figure further shows the potential energy surface for the S4 system (notation as in Figure 3) in the trilayer system, as well as the value obtained by doubling the bilayer interaction energy for the same adsorption pattern. As is immediately clear from the close agreement between the two curves, there is little interaction between the top- and bottom-BN layer. The energy difference at the minimum of the curves is indeed ≈4.5 meV or 2.8% of the total interaction energy. In order to further verify this result, the plot also shows the PES at the HF- and the LMP2-level for the same trilayer system where all the atoms in the Graphane layer have been transformed into ghosts. Interestingly, even given the large charge-separation within the BN-layer, HF-contributions play virtually no role in the BN–BN interaction with LMP2-contributions dominating. Still the absolute value of the

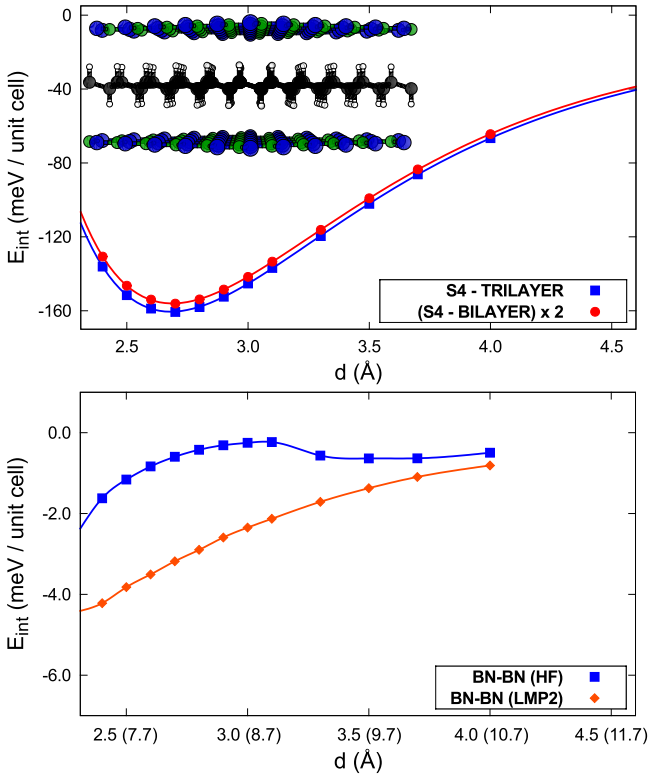

FIG. 5. The top-figure shows the HF + LMP2 – PES for the S4 trilayer system as well as the curve obtained by doubling the S4 bilayer interaction energy. The bottom-figure on the other hand shows HF and LMP2 contributions to the pure BN–BN interaction energy for the same system where atoms in the Graphane sheet have been transformed into ghosts. The interlayer distance shown on the x-axis refers to the same distance indicated in the top-figure, while the corresponding BN–BN distance is indicated in parenthesis. A structural model of the BN/Graphane/BN trilayer system is shown in the inset of the top-figure for clarity.

contributions remains small which is to be expected due to the large BN–BN interlayer spacing. Upon comparing the two figures we notice that the differences between the multilayer binding curves are smaller than the BN–BN interaction energy. This is likely due to partial screening of the BN–BN interaction by the Graphane sheet as well as small artifacts arising from the chosen method of BSSE correction (see supplementary material[32]).

To summarize this part, while the interaction between the Graphane and the BN has been shown to be dispersive in nature, the preference of the Graphane for different BN-adsorption sites is caused by static repulsion mainly attributable to the N-atom. We further showed how, even given the large partial charges within the BN-layer, net electrostatic interaction between two BN-layers in a BN/Graphane/BN trilayer structure is insignificant, and the interaction energies between BN-sheets on opposite sites of the Graphane layer are largely additive in the trilayer system.

B. The effect of external-electric fields

As briefly mentioned in the Introduction, the effect of an external electric field has been addressed in the literature, mainly due to the potential use of electric fields for controlling the bonding of molecular hydrogen to BN substrates.[20] Our discussion here will focus on the band structures, dipole

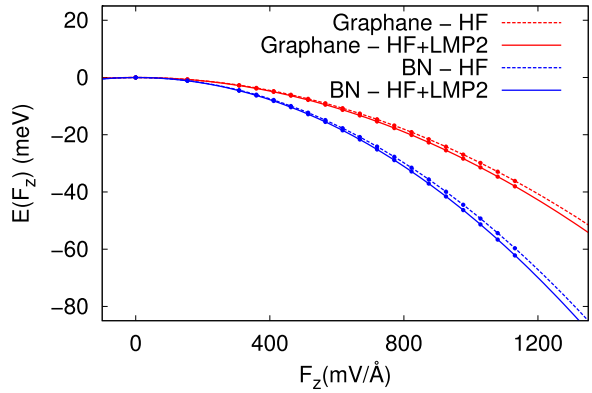

FIG. 6. Energy ($E(F_z)$) of an isolated BN and Graphane sheet as a function of the external electric field. Points show the results from the *ab-initio* calculations, while the lines where obtained by fitting a second order polynomial to the *ab-initio* data. Dashed and full lines indicate results at the HF- and LMP2-level of theory, respectively. For convenience, E_0 as defined in Eq. (1) has been set to 0 in all cases.

moments and polarizabilities of BN and Graphane, and how these properties are affected by multi-layering as well as the respective role of HF- and LMP2 contributions.

The change in the energy E of a system as a function of an external electric field along the z-direction (F_z) can be expressed as a Taylor-type series in the field as

$$E(F_z) = E_0 - \mu_z F_z - \frac{1}{2}\alpha_{zz}F_z^2 + \cdots, \quad (1)$$

where E_0 is the energy of the system at zero-field, μ_z is its dipole moment along the z-direction, and α_{zz} the diagonal component of the polarizability tensor along the same direction. Note that for consistency we will always use meV as well as Å as units of energy and length, respectively. μ is therefore given in units of $e \cdot$ Å ≈ 1.890 a.u., where e is the elementary charge, while α will be given in units of Å^3. The polarizability units do not correspond to the direct results of the fitting procedure (eÅ^2/mV) but were chosen for both ease of conversion to the commonly used polarizability volume given in units of a_0^3 as well as the convenient numerical values they yield.

Figure 6 shows $E(F_z)$ for both the isolated BN as well as the isolated Graphane sheet. Two curves are shown for each system, corresponding to pure HF as well as total LMP2 energy. As can be seen from Figure 6, correlation-contributions to the polarizability are very small at low to moderate field intensities in both cases and become relevant only at high field strengths around ≈800 mV/Å. Upon second-order polynomial fit of the data shown in Figure 6, values for α_{zz} can be obtained and the results are shown in Table I. Note that μ_z is zero for both BN as well as Graphane.

TABLE I. Polarizability (α_{zz}) values for an isolated BN and Graphane sheet, respectively, as obtained from a second-order polynomial fit of the data shown in Figure 6. Values are given in Å^3.

	Graphane		BN	
	HF	HF+LMP2	HF	HF+LMP2
α_{zz}	1.34	1.40	0.81	0.86

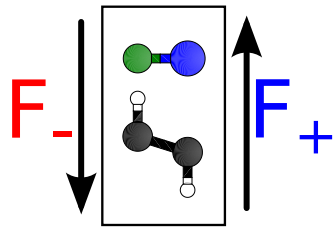

FIG. 7. F_+ and F_- field-orientations for the Graphane/BN bilayer system as used throughout this work.

TABLE II. Dipole moments (μ_z) and polarizability (α_{zz}) values for the bilayer and trilayer S2 and S4 systems as well as isolated BN and Graphane sheets, respectively, as obtained from a second-order polynomial fit of the data shown in Figure 8. Values for polarizabilities are given in Å^3 while dipole moments are given in units of Å $\cdot e$.

	S2		S4			
	BL	TL	BL	TL	Graphane	BN
μ_z	0.003	0.000	0.002	0.000	0.000	0.000
α_{zz}	2.28	3.14	2.27	3.12	1.40	0.86

If we now move from the simple monolayer to the bilayer system, an interesting effect occurs. We will focus here on the S2 and the S4 systems as the S4 system shows the strongest binding, while the S2 system shows almost identical binding to the S3 system while retaining the same B adsorption site as present in the S4 case. The discussion for other systems proceeds along parallel lines. The application of an external electric field introduces directionality along the surface-normal causing the existence of two different types of adsorption for each of the six systems. The two orientations are indicated as F_+ and F_-, respectively, and shown schematically in Figure 7. As seen in Figure 8, the two orientations show significantly different binding energies as their dipole moment (see Table II) is either aligned or anti-aligned with the field.

While this effect of the dipole alignment/anti-alignment can very clearly be seen from the right-hand side of Figure 8, the binding energy curves on the left-hand side do not show an equal energy change for the two field directions with respect to the zero-field case. The origin of this difference lies in the combined effect of dipole alignment/anti-alignment and the polarizability of the system, which almost perfectly cancel out for the F_- case at the electric field strength used for the PES-calculations.

Figure 8 also shows the results obtained from introducing a second BN layer into the system. As explained above, we have only considered the case in which the second BN layer is connected to the first by inversion symmetry. This has the consequence of again forcing the dipole moment of the system to be zero by symmetry. As seen from comparing the curves for the bilayer- and trilayer-systems, the non-zero dipole moment

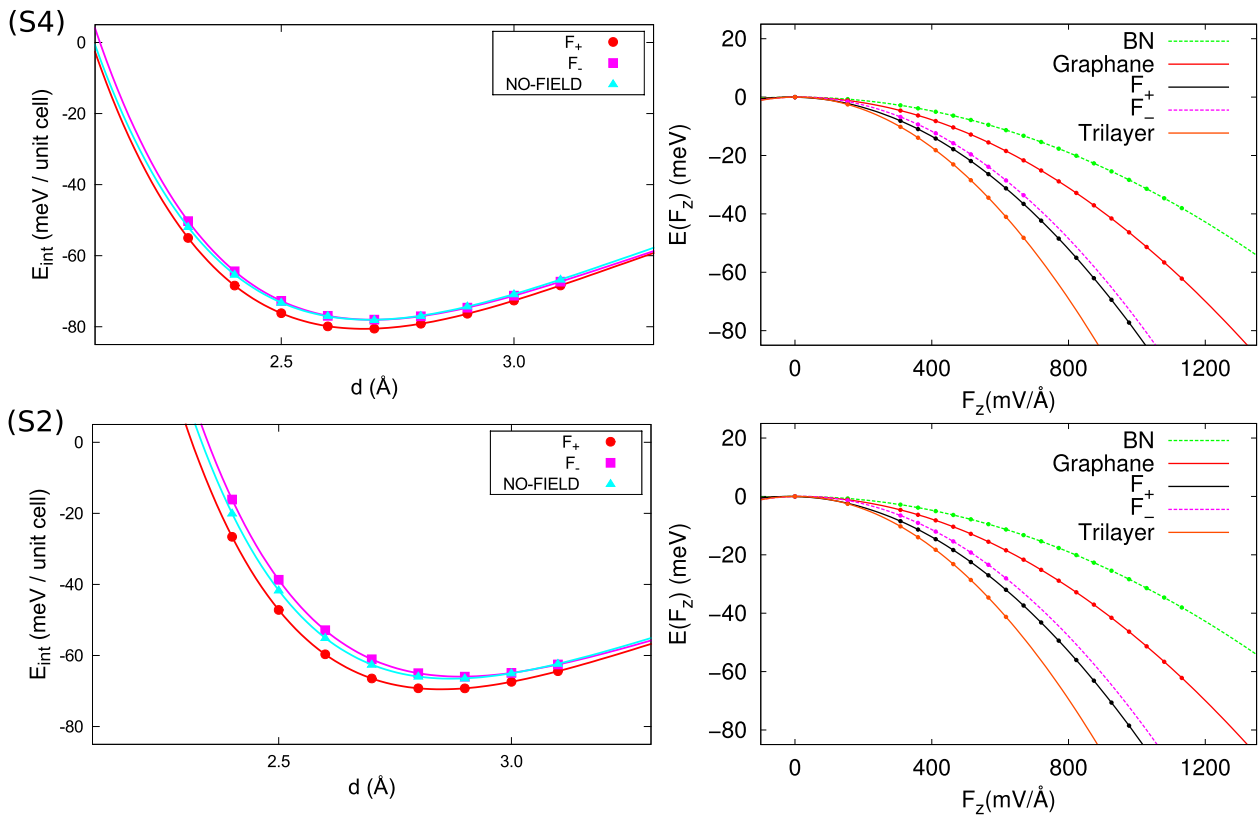

FIG. 8. PES and electric field response for the S4 and the S2 systems. The left-hand figures show the potential energy curve for the respective bilayer system under an external electric field of 514 mV/Å. Both the F_+ and F_- field orientations as defined in Figure 7 as well as the field-free (NO-FIELD) case are shown. The right-hand figures on the other hand show the energy ($E(F_z)$) (at the LMP2-level) of these same systems as a function of the external electric field, calculated at the equilibrium distance at zero-field, as well as the corresponding curve for the trilayer systems (Trilayer). For comparison, the data for an isolated Graphane and BN sheet as seen in Figure 6 are also shown. Points indicate the results from the *ab-initio* calculations, while the lines were obtained by fitting a second order polynomial to the *ab-initio* data. For convenience, E_0 has been set to 0 in all cases.

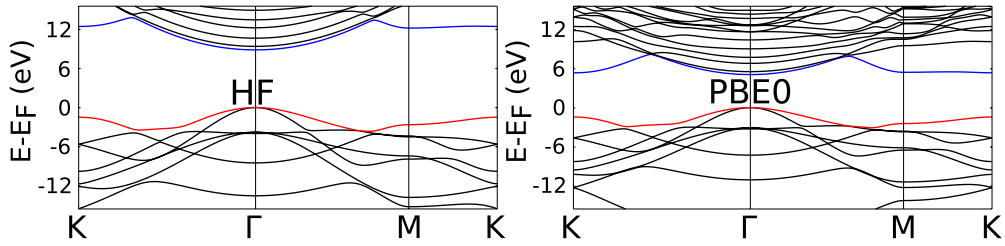

FIG. 9. HF and PBE0 band structures and projected DOS for the S4 bilayer system. The bands forming the VBM and CBM have been color-coded in red and blue, respectively, for emphasis.

of the bilayer system is too weak to dominate the response, compared to the higher polarizability of the trilayer system (≈3.1 for the trilayer vs. ≈2.3 for the bilayer system) even at low field values.

The weak nature of the interlayer binding now leads us to suspect that polarizabilities, just as the aforementioned binding energies, should largely be additive. Indeed, we see from Table II that $\alpha_{zz}(\text{Bilayer}) \approx \alpha_{zz}(\text{BN}) + \alpha_{zz}(\text{GrH})$ and $\alpha_{zz}(\text{Trilayer}) \approx \alpha_{zz}(\text{GrH}) + 2 \times \alpha_{zz}(\text{BN})$.

It is clear from the above discussion that, while binding in all structures is mainly due to dispersive interactions, as in the system's preference for adsorption-sites, its response to an external electric field is largely captured at the HF-level with correlation at the LMP2-level providing only small corrections.

To conclude let us now discuss the effect of the application of an external electric field on the band structure of the S4 system. As HF is known to overestimate band gaps, band structure calculations have been performed using the PBE0 hybrid functional. To show the effect of this choice of method, Figure 9 shows the zero-field band structure of the S4-system as calculated by both HF as well as PBE0. Apart from the above-mentioned reduction in band gap, the most striking difference between the two band structures is the reduction in the energy-splitting between the lowest unoccupied states at Γ and K/M, respectively, whereas the dispersion-behavior of the occupied bands is only slightly altered.

Let us now consider the effect of applying an external electric field. PBE0-band structure plots for the S4 bilayer system in both the F_- and F_+ cases (see Figure 7) as well as the field-free case are shown in Figure 10. The plot further indicates projected DOS for the Graphane and BN contributions as well as the ghost-atoms used to improve the virtual-space description. Upon considering the projected DOS in the top-image in Figure 10, we indeed notice the large contribution of the ghost atoms to the virtual bands of

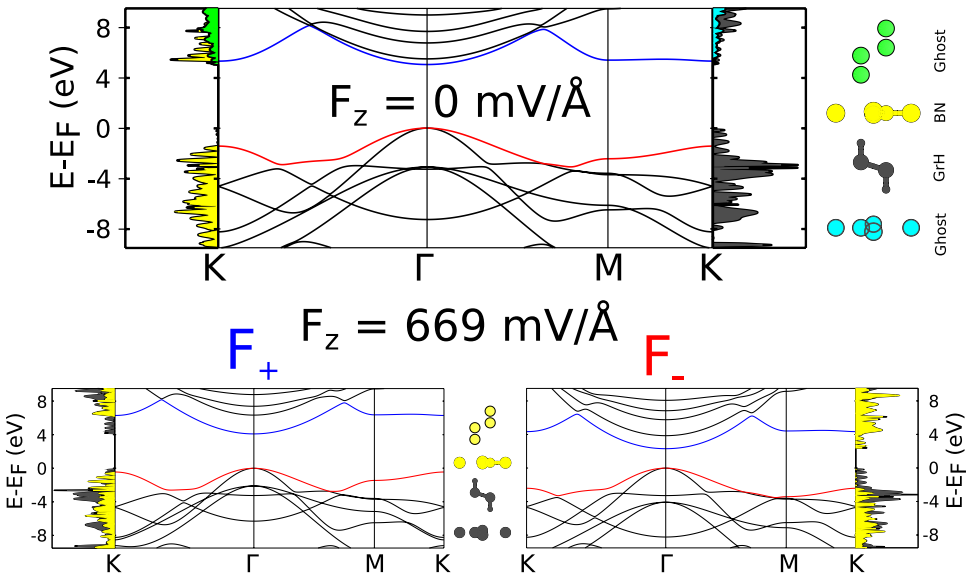

FIG. 10. PBE0-band structures for the S4 system in the field-free case as well as under an external electric field of 669 mV/Å. For the field-free case (top), projected DOS are shown on the both sides of the band structure plot with the left-hand side corresponding to BN (yellow) and ghost-Graphane (green) contributions and the right-hand side indicating Graphane (gray) as well as ghost-BN projections (turquoise) of the DOS. In the bottom plots, contribution from ghost-atoms has been added to the associated atoms and indicated in yellow (BN) and gray (Graphane), respectively. In all cases the bands forming the VBM/CBM have been color-coded in red/blue, respectively, for emphasis.

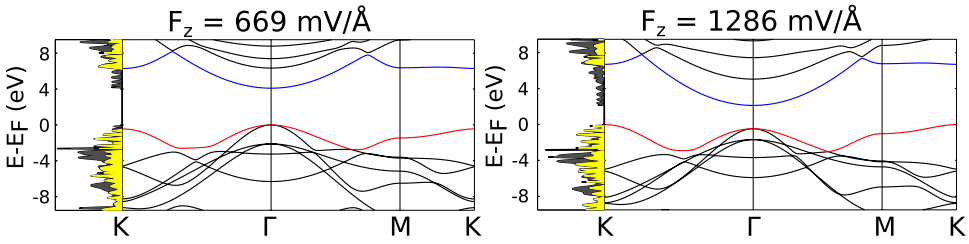

FIG. 11. PBE0-band structures for the S4-bilayer system for an external field of 669 meV/Å and 1286 meV/Å respectively, applied along the F_+-direction. Local DOS are shown for both cases and refer to projections on Graphane (gray) and BN (yellow) atoms including ghost atoms (see Figure 10).

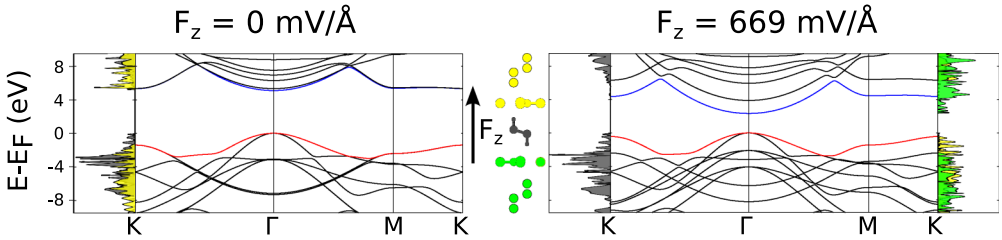

FIG. 12. PBE0-band structures for the S4-trilayer system in the field-free case and under an external field of 669 meV/Å respectively. Local DOS are shown for both cases and refer to projections on Graphane (gray) and BN (yellow/green) atoms including ghost atoms as shown in the central figure where the direction of the external field has further been indicated. For the field-free case, only one set of projections is shown as both sides are symmetry-equivalent.

both Graphane as well as BN. While isolated Graphane has a direct-Γ-centered band gap and monolayer BN shows an indirect, K → Γ gap, the S4 system shows a direct Γ → Γ gap, associated with a Graphane to BN charge transfer. Note that the conduction-band minimum (CBM) located on the BN-layer lies only slightly lower in energy than the lowest-energy Graphane-band at the Γ-point.

The picture changes though when an external electric field is applied. For the F_+ field-direction, the field causes BN-bands to shift upwards in energy. For fields up to ≈669 meV/Å, this causes the CBM to shift from BN to Graphane, while the VBM remains located on the Graphane-layer. The band gap of the S4-system is thereby changed from a Graphane-BN charge transfer to a Graphane-centered gap. For fields stronger than ≈669 meV/Å, BN-bands at the K-point move above the Graphane VBM at Γ and the band gap shifts to an indirect K → Γ gap with the direction of the charge transfer being reversed with respect to the zero-field case (see Figure 11). If the field is applied in the F_- direction on the other hand, BN-bands are shifted down in energy, causing no change in band-gap character but a stronger splitting of the conduction bands.

Finally, let us consider the effect of an external field on the trilayer band structure. Figure 12 shows the S4-PBE0 trilayer band structure in both the field-free case as well as under an external field of 669 meV/Å. In the zero-field case, the same behavior as in the bilayer is observed with the band gap corresponding to a Graphane-BN charge transfer transition at the Γ-point. As an external field is applied, both effects seen in the bilayer-cases combine leading to a spreading of the conduction bands as well as an upwards-shift of the K-point occupied BN-bands moving them closer to the VBM, located on the Graphane-layer. Even stronger fields could accordingly be used to induce a BN–BN charge transfer for the trilayer-system band gap created between K and Γ with the direction of the charge transfer being controlled by the direction of the external field.

IV. CONCLUSIONS

Herein, we have presented the to the best of our knowledge first full *ab-initio* study of combined Graphane/BN structures and their response to static external electric fields applied along the surface-normal direction.

We have shown how HF/LMP2 calculations can be applied to gain a detailed understanding of the effects causing preferential binding sites in terms of relative contributions from static repulsion and electron correlation. We have further demonstrated the effects of multilayering of the aforementioned systems on their polarizability as well as the consequences of an external electric field on the interaction energy of these multilayered structures.

Finally, we investigated the effects of an external electric field on the band structures of Graphane/BN bilayer system. While the band gap has the character of a direct Γ-centered gap associated with a Graphane to BN charge transfer in the field-free case, the application of an external electric field allows to shift the gap to a Graphane-centered gap and subsequently to an indirect K → Γ gap associated with a BN to Graphane charge transfer, depending on the field strength. Finally, in the trilayer case, the external field can induce a BN–BN charge transfer between the BN-layers located on either side of the Graphane-layer; the direction of this charge transfer can be controlled by the direction of the external field.

ACKNOWLEDGMENTS

The authors would like to thank L. Hammerschmidt and A. Achazi (both Berlin) for enlightening discussions. The High Performance Computing Network of Northern Germany (HLRN) and computer facilities of the Freie Universität Berlin (ZEDAT) are acknowledged for computer time. LEMS further acknowledges the financial support by the International Max Planck Research School "Complex Surfaces in Material Sciences" as well as Victoria University of Wellington. The authors appreciate the support from the German Research Foundation (DFG) through the Priority Program 1459 (Graphene). The XCrySDen program[37] was used to create images of atomic structures throughout this work.

[1]K. S. Novoselov, A. K. Geim, S. Morozov, D. Jiang, Y. Zhang, S. Dubonos, I. Grigorieva, and A. Firsov, Science **306**, 666 (2004).
[2]A. K. Geim and K. S. Novoselov, Nat. Mater. **6**, 183 (2007).
[3]A. K. Geim, Science **324**, 1530 (2009).
[4]R. Mas-Balleste, C. Gomez-Navarro, J. Gomez-Herrero, and F. Zamora, Nanoscale **3**, 20 (2011).
[5]M. Engler, C. Lesniak, R. Damasch, B. Ruisinger, and J. Eichler, *CFI* (Göller, 2007), Vol. 84.
[6]G. Giovannetti, P. A. Khomyakov, G. Brocks, P. J. Kelly, and J. van den Brink, Phys. Rev. B **76**, 073103 (2007).
[7]R. Quhe, J. Zheng, G. Luo, Q. Liu, R. Qin, J. Zhou, D. Yu, S. Nagase, W.-N. Mei, Z. Gao *et al.*, NPG Asia Mater. **4**, e6 (2012).
[8]J. Sławińska, I. Zasada, P. Kosiński, and Z. Klusek, Phys. Rev. B **82**, 085431 (2010).
[9]H. Wang, T. Taychatanapat, A. Hsu, K. Watanabe, T. Taniguchi, P. Jarillo-Herrero, and T. Palacios, IEEE Electron Device Lett. **32**, 1209 (2011).

[10]I. Meric, C. Dean, A. Young, J. Hone, P. Kim, and K. L. Shepard, in *Electron Devices Meeting (IEDM), 2010 IEEE International* (IEEE, 2010), p. 23.2.1.
[11]A. Ramasubramaniam, D. Naveh, and E. Towe, Nano Lett. **11**, 1070 (2011).
[12]J. O. Sofo, A. S. Chaudhari, and G. D. Barber, Phys. Rev. B **75**, 153401 (2007).
[13]M. Linnolahti, A. J. Karttunen, and T. A. Pakkanen, ChemPhysChem **7**, 1661 (2006).
[14]M. H. Sluiter and Y. Kawazoe, Phys. Rev. B **68**, 085410 (2003).
[15]D. Elias, R. Nair, T. Mohiuddin, S. Morozov, P. Blake, M. Halsall, A. Ferrari, D. Boukhvalov, M. Katsnelson, A. Geim *et al.*, Science **323**, 610 (2009).
[16]X. Blase, A. Rubio, S. G. Louie, and M. L. Cohen, Phys. Rev. B **51**, 6868 (1995).
[17]F. Karlický and M. Otyepka, J. Chem. Theory Comput. **9**, 4155 (2013).
[18]B. Gharekhanlou, S. Tousaki, and S. Khorasani, J. Phys.: Conf. Ser. **248**, 012061 (2010).
[19]G. Fiori, S. Lebegue, A. Betti, P. Michetti, M. Klintenberg, O. Eriksson, and G. Iannaccone, Phys. Rev. B **82**, 153404 (2010).
[20]J. Zhou, Q. Wang, Q. Sun, P. Jena, and X. Chen, Proc. Natl. Acad. Sci. U. S. A. **107**, 2801 (2010).
[21]J. T. Tanskanen, L. Maschio, A. J. Karttunen, M. Linnolahti, and T. A. Pakkanen, ChemPhysChem **13**, 2361 (2012).
[22]E. Voloshina, D. Usvyat, M. Schütz, Y. Dedkov, and B. Paulus, Phys. Chem. Chem. Phys. **13**, 12041 (2011).
[23]M. Halo, S. Casassa, L. Maschio, C. Pisani, R. Dovesi, D. Ehinon, I. Baraille, M. Rérat, and D. Usvyat, Phys. Chem. Chem. Phys. **13**, 4434 (2011).
[24]M. Halo, C. Pisani, L. Maschio, S. Casassa, M. Schütz, and D. Usvyat, Phys. Rev. B **83**, 035117 (2011).
[25]G. Constantinescu, A. Kuc, and T. Heine, Phys. Rev. Lett. **111**, 036104 (2013).
[26]R. Dovesi, R. Orlando, B. Civalleri, C. Roetti, V. R. Saunders, and C. M. Zicovich-Wilson, Z. Kristallogr. **220**, 571 (2005).
[27]R. Dovesi, V. R. Saunders, C. Roetti, R. Orlando, C. M. Zicovich-Wilson, F. Pascale, B. Civalleri, K. Doll, N. M. Harrison, I. J. Bush, P. D'Arco, and M. Llunell, *CRYSTAL09 User's Manual* (University of Torino, Torino, 2009).
[28]C. Pisani, L. Maschio, S. Casassa, M. Halo, M. Schütz, and D. Usvyat, J. Comput. Chem. **29**, 2113 (2008).
[29]C. Pisani, M. Schütz, S. Casassa, D. Usvyat, L. Maschio, M. Lorenz, and A. Erba, Phys. Chem. Chem. Phys. **14**, 7615 (2012).
[30]S. S. Erba A and M. Halo, *CRYSCOR09 User's Manual* (University of Torino, Torino, 2014), www.cryscor.unito.it.
[31]S. F. Boys and F. d. Bernardi, Mol. Phys. **19**, 553 (1970).
[32]See supplementary material at http://dx.doi.org/10.1063/1.4917170 for details regarding basis set, BSSE-correction as well as CRYSTAL/CRYSCOR input parameters.
[33]J. W. Boughton and P. Pulay, J. Comput. Chem. **14**, 736 (1993).
[34]R. Pease, Nature **163**, 722 (1950).
[35]C. Adamo and V. Barone, J. Chem. Phys. **110**, 6158 (1999).
[36]M. F. Peintinger, D. V. Oliveira, and T. Bredow, J. Comput. Chem. **34**, 451 (2013).
[37]A. Kokalj, Comput. Mater. Sci. **28**, 155 (2003).